Spin Dynamics and Relaxation in Graphene Nanoribbons: Electron Spin Resonance Probing

Singamaneni S. Rao,[†,¶,*] Andre Stesmans,[†] Johan van Tol,[‡] Dmitry V. Kosynkin,[§] A. Higginbotham-Duque,[§] Wei Lu,[§] Alexander Sinitskii,[§] and James. M. Tour[§,⊥,‖]

[†]INPAC, Institute for Nanoscale Physics and Chemistry, Semiconductor Physics Laboratory, K.U. Leuven, Celestijnenlaan 200D, B-3001 Leuven, Belgium, [‡]National High Magnetic Field Laboratory, Centre for Interdisciplinary Magnetic Resonance, Florida State University, 1800 East Paul Dirac Drive, Tallahassee, Florida 32310, United States, and [§]Department of Chemistry, [⊥]Department of Mechanical Engineering and Materials Science, and [‖]Smalley Institute for Nanoscale Science and Technology, Rice University, MS-222, 6100 Main Street, Houston, Texas 77005, United States. [¶]Present address: Materials Science Division, Army Research Office, Research Triangle Park, North Carolina 27709, United States, and Department of Material Science and Engineering, North Carolina State University, Raleigh, North Carolina 27695, United States

ABSTRACT

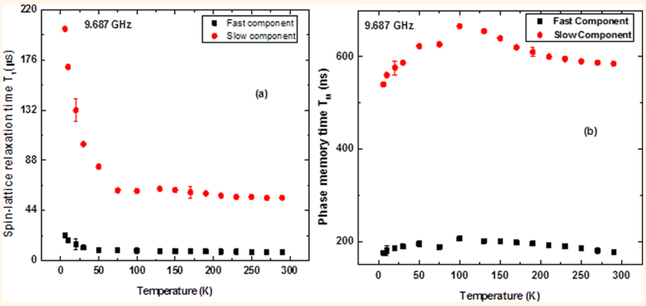

Here we report the results of a multifrequency (∼9, 20, 34, 239.2, and 336 GHz) variable-temperature continuous wave (cw) and X-band (∼9 GHz) pulse electron spin resonance (ESR) measurement performed at cryogenic temperatures on potassium split graphene nanoribbons (GNRs). Important experimental findings include the following: (a) The multifrequency cw ESR data infer the presence of only carbon-related paramagnetic nonbonding states, at any measured temperature, with the *g* value independent of microwave frequency and temperature. (b) A linear broadening of the ESR signal as a function of microwave frequency is noticed. The observed linear frequency dependence of ESR signal width points to a distribution of *g* factors causing the non-Lorentzian line shape, and the *g* broadening contribution is found to be very small. (c) The ESR process is found to be characterized by slow and fast components, whose temperature dependences could be well described by a tunneling level state model. This work not only could help in advancing the present fundamental understanding on the edge spin (or magnetic)-based properties of GNRs but also pave the way to GNR-based spin devices.

KEYWORDS: electron spin relaxation rate · graphene nanoribbons · tunneling level states · electron spin resonance · edge spin

Graphene has emerged as a promising and versatile material, with outstanding electronic and spintronic properties that could be useful in many device applications, owing to its high carrier mobility and long spin lifetime resulting from low spin–orbit coupling (SOC) (∼10^{-4} eV) and low hyperfine (hf) interaction.[1−3] Recently, the demonstration of room temperature electron spin transport and spin precession in single-layer graphene (SLG),[4] discovery of a large band gap[5] in graphene nanoribbons (GNRs), and the observation of room temperature long relaxation times (∼2 ns) and coherence lengths (∼0.7 μm) in bilayer graphene (BLG)[6] have suggested that graphene-based materials could play a pivotal role in spintronic devices that manipulate electron spin rather than charge. In particular, zigzag GNRs (ZGNRs) have magnetic (spin) states at their edges, and these states can be antiparallel or parallel and are prone to external stimuli.

As mentioned above, long spin relaxation times and phase coherence lengths in graphene are expected, which are based on the weak atomic SOC in carbon ($Z = 6$). However, a recent spin injection measurement[4,6−8] based on a "nonlocal spin valve geometry" revealed surprisingly short spin relaxation times of only about 100−200 ps. However, spin relaxation times are reported to be weakly dependent on the charge density and temperature. These results appear puzzling, although the low mobilities of the samples (about 2000 $\text{cm}^2/(\text{V}\cdot\text{s})$) suggest that the measured spin relaxation times are likely due to extrinsic effects such as the substrate and contact of graphene with external electrodes. As rightly discussed in recent theoretical work,[9] spin relaxation in graphene can be governed by the corrugations (ripples) of graphene, the exchange interaction with local magnetic moments, SOC-mediated relaxation as well as the effect of the underlying substrate. In that work, the authors have inferred that the charged impurities in the substrate and remote surface phonons are relevant for the spin relaxation and mobility in graphene.

So far, in spin-valve experiments on graphene, metallic electrodes were deposited

* Address correspondence to ssingam@ncsu.edu.

Received for review December 5, 2011 and accepted August 17, 2012.

10.1021/nn302745x

to realize working tunnel barrier contacts. This likely brings in additional SOC leading to unrealistic relaxation times, obscuring their true intrinsic nature. To probe the intrinsic spin relaxation, one should work with ribbons free from substrate effects, metallic electrodes, and charged impurities. Therefore, the technique of choice is pulse electron spin resonance (ESR) spectroscopy. As suggested by the recent theoretical analysis[10] of spin relaxation time in graphene, it was concluded that the spin relaxation in graphene is neither due to the Elliott−Yafet nor due to the Dyakonov−Perrel mechanism. Indeed, the authors in that reference have suggested to employ ESR spectroscopy to assess the true magnitude of the electron spin relaxation time.

Having realized the potential advantages of GNRs, with innovative chemical methods, high-quality GNRs have been produced[11,12] in bulk quantities through potassium splitting or oxidative unzipping of multiwalled carbon nanotubes (MWCNTs). During the splitting or unzipping MWCNT process, if paramagnetic defect centers are induced by the fragmentation of C−C chemical bonds, characteristic ESR signals should be observed.[13−15] If the GNR applications are to succeed, a thorough understanding of electrically/magnetically active point defects at the edges/graphene fragments is required. ESR spectroscopy is a powerful technique to probe unpaired electron spins in paramagnetic materials and has been applied to pure graphite[16] and carbon nanotubes.[17] From the analysis of the ESR signals, the concentration of unpaired electrons, their chemical distinction, and molecular structure and the reactivity of such radicals may be clarified and investigated. In carbon-based materials, ESR can discriminate between localized and itinerant electrons.

The objective of the present work is to address the nature of edge spins and spin dynamics in detail through a broad multifrequency continuous wave (cw) and pulse ESR spectroscopy study carried out on pristine GNRs. Our experimental investigations led to spin relaxation times on the order of microseconds. It was also discovered that spin relaxation times are strongly temperature-dependent unlike the weak temperature dependence theoretically predicted.[9] The current work concludes that the spin relaxation times are found to be governed by a tunneling level state (TLS)-type relaxation process, typically employed for disordered solids in which the defect paramagnetic centers are not strongly bound to the main phonon bath (see below), indicating that the phonon contribution is minimal in free-standing GNRs. On the basis of these data, we can rule out unwanted contributions emanating from charged impurities that might be present in a substrate (causing strong impurity Coulomb scattering to the spin relaxation rate) as these ribbons are free-standing, without being supported by an underlying substrate.

RESULTS AND DISCUSSION

Multifrequency Continuous Wave ESR. Figure 1a−e displays ESR signals measured at various microwave frequencies (8.91, 20.60, 34, 239.2, and 336 GHz) collected at 10 K on GNRs. The sharp signal seen in Figure 1a−c appearing at $g = 1.99869 \pm 0.00002$ is due to the co-mounted Si:P marker. For all three low frequencies (8.91, 20.60, and 34 GHz), ESR detected only one isotropic, non-Lorentzian ESR signal (see Supporting Information), appearing at $g \sim 2.0032$. This value falls within the reported[13−15] carbon ESR signal range (g = 2.0022−2.0035), indicating that the signal may be ascribed to C-related dangling bonds of spin $S = 1/2$. This narrow peak observed close to the free-electron g value ($g \sim 2.0023$) is a characteristic of the localized spins of the edge state.[13−15] In an effort to unravel the origin and location of the ESR signal detected from the ribbons, we have done extensive investigation, as disclosed in our recent work.[13] From the detailed ESR work coupled with kinetic study,[13] under various gas environments and as a function of time and temperature, it has been inferred that, most likely, the ESR signal originates from the edges of the ribbons. By means of tilted magnetic field experiments, and by applying the Lifshitz−Kosevich formula, Kurganova and co-authors have reported[20] an exchange-induced g factor (enhancement) of $g = 2.7 \pm 0.2$ for both single-layer and bilayer graphene, attributed to many-body interactions. The apparent discrepancy in g value may either arise from the fact that the transport measurements[20] consider many-body effects looking at charged (dressed) spins or be due to an entirely different spin entity. However, the conventional ESR spectroscopy provides the g value of bare spins by neglecting many-body effects.

Through numerical double integration of detected first derivative ESR signal measured at K-band and at 4.2 K with respect to the co-mounted Si:P marker sample, the spin density for GNRs is estimated at $\sim 6 \times 10^{19}$ g^{-1}. Detailed information and discussion has been disclosed in our earlier work[14,15] as well.

Despite intense signal averaging over broad field ranges under various extreme and optimized spectrometer parameter settings, no other ESR signals could be observed. Though intensely searched for, no correlated additional signal structure could be traced nor was there any sign of hyperfine (hf) structure possibly ensuing from highly abundant ^{1}H and ^{39}K nuclei. The non-Lorentzian line shape suggested the existence of either a very complex spin correlation function in the exchange-coupled system or a superposition of several different overlapping components. In the section below, we discuss our pulsed ESR measurements, which were conducted in order to elucidate this matter.

With the aim of resolving the origin of the non-Lorentzian line shape, unlike the Lorentzian shape ESR

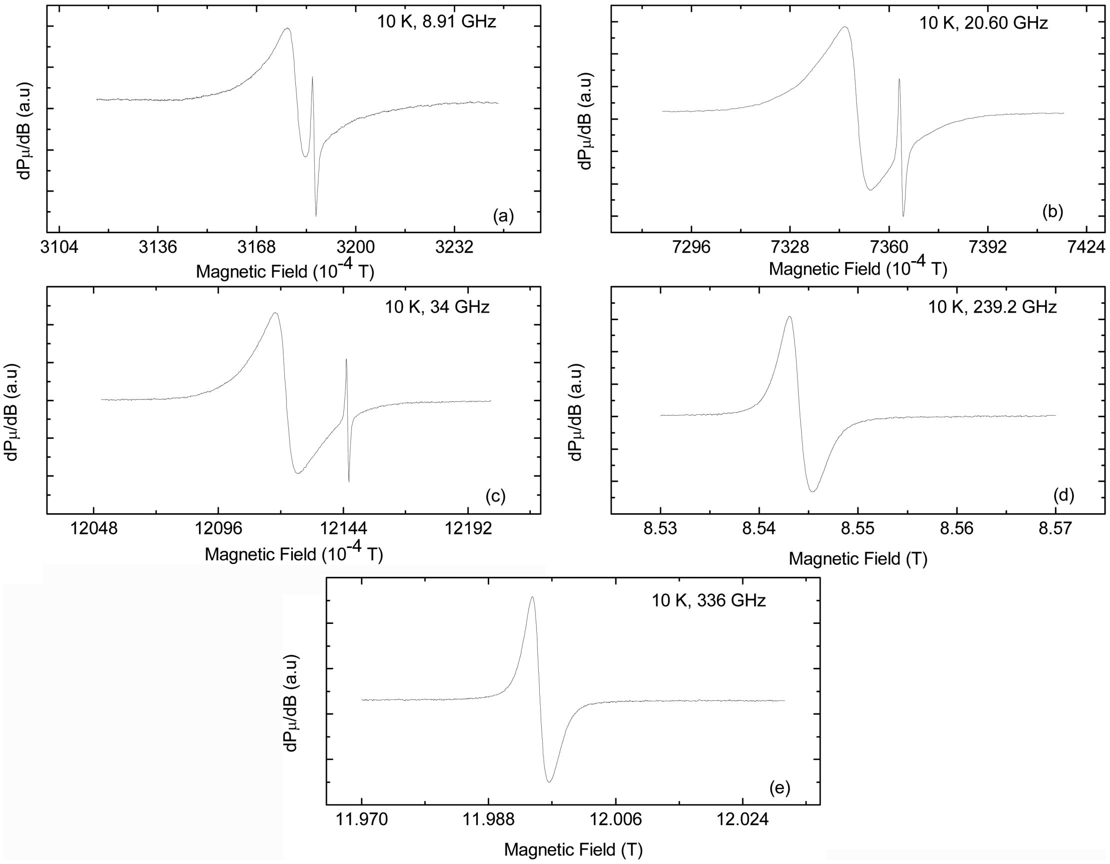

Figure 1. Conventional first derivative cw ESR spectra measured on GNRs at 10 K, at the microwave frequency of (a) 8.91 GHz (X-band), (b) 20.60 GHz (K-band), (c) 34 GHz, (d) 239.2 GHz, and (e) 336 GHz. The signal at $g \approx 1.99869$ (a–c) stems from a co-mounted Si:P marker sample. For the first three spectrometers, the modulation field used was $B_m = 0.42 \times 10^{-4}$ T and the microwave power was $P_\mu = 2.5$ nW. At high frequency (d,e), the modulation field used was $\sim 10^{-4}$ T and the microwave power was $P_\mu = 20$ μW.

signal observed[13−15] from chemically converted graphene nanoribbons (CCGNRs), we measured the ESR signal from GNRs at two additional high microwave frequencies, 239.2 and 336 GHz at 10 K. As displayed in Figure 1d,e, we did not observe more than one ESR signal nor did we observe any significant *g* shift from the free electron *g* value (2.0023) at any measured frequency. A single signal was detected at the two high frequencies measured, and just a linear increase of width with the frequency (*f*) is observed. Such a non-Lorentzian ESR line shape has been reported in other carbon-based materials such as peapods[21] measured up to 420 GHz and in carbon nanofoam samples.[22]

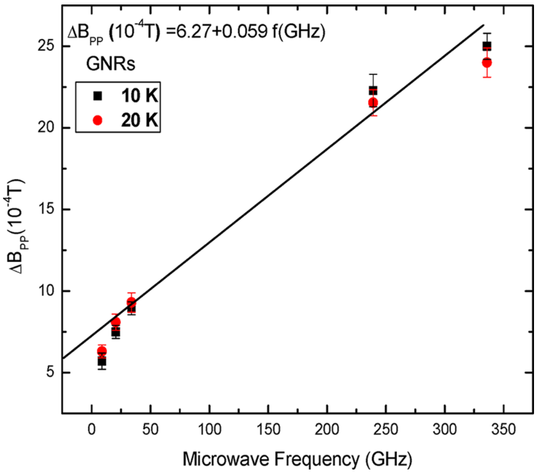

Figure 2. Microwave frequency (*f*) dependence of ΔB_{PP} of GNRs at 10 and 20 K. A linear frequency dependence was observed, suggesting a strain-induced spread in *g* as a limited line broadening (0.059 f(GHz)10^{-4} T) mechanism, with a large *f*-independent part of 6.27 × 10^{-4} T. The solid lines represent a least-squares linear fit, described by ΔB_{PP} (10^{-4} T) = 6.27 + 0.059*f* (GHz).

As plotted in Figure 2 (at 10 and 20 K), the peak-to-peak ESR signal width ΔB_{PP} is found to be linearly dependent on microwave frequency (*f*). From least-squares computer fitting of the experimental data, the obtained *f*-dependent part ΔB^{f}_{PP} is 0.059 × 10^{-4} T/GHz (at 10 and 20 K), which is a Gaussian part, though it is found to be rather small compared to the frequency-independent part (6.27 × 10^{-4} T). This Gaussian part can be attributed to a *g* distribution effect resulting from different local environments of paramagnetic centers in GNRs. The remaining *f*-independent part can be due to dipolar interaction or unresolved hyperfine (hf) interaction—perhaps, arising from hydrogen nuclei—resulting in inhomogeneous Gaussian broadening;

there may also be a contribution from molecular oxygen. However, in our recent work[13] on CCGNRs, we found that molecular oxygen does not broaden the ESR signal width. Similarly, even in GNRs, we believe that the effect of molecular oxygen on the ESR line width is negligible. Then, the main contribution may arise from the unresolved hf coupling to protons. The explicit evidence for the presence of protons in GNRs has been shown in our HYSCORE measurements as discussed in our previous work.[15]

Now, we discuss the thermal evolution of ESR signals measured from GNRs. Representative first derivative X-band (~8.91 GHz) continuous wave ESR signals collected from GNRs are shown in Figure 3a as a function of temperature (7, 30, 50, and 90 K). The signal at $g = 1.99869 \pm 0.000\,02$ stems from a co-mounted Si:P marker. All of the signals were recorded under the same experimental conditions, except for the temperature. As one can immediately notice from Figure 3b, the signal intensity appears to decrease as the temperature increases according to the Curie-type behavior; also, a weak temperature dependence of line width is observed—a typical signature of localized electronic states. Such signatures have been observed previously[14] for CCGNRs, as well. For the conduction electron spins to be detected, the ESR signal intensity is expected to be independent of temperature. In addition, for conduction electrons, the ESR signal width increases as the temperature increases, in accordance with the well-known Elliott mechanism.[23] Several such ESR studies have been reported[24,25] on carbon-based materials to reveal the presence of a conduction electron. Apparently, such signatures are found to be absent in our GNRs as well as in CCGNRs.[14] In addition, we have recorded ESR signals from pristine MWCNTs as well as fresh HOPG (highly oriented pyrolytic graphite) as a function of temperature. Our data revealed typical signatures of conduction electrons from these two samples (MWCNTs and HOPG) as one might anticipate. We have disclosed such information in our earlier report.[14] Also, the presence of localized states could be inferred from our transport data, as well,[12] which was explained using a variable range hopping (VRH) mechanism,[12,14] typically used for disordered systems of localized states. In addition, the transmission electron microscope (TEM) image published in our earlier report[12] on the ribbons (CCGNRs) reveals a nonuniform structure resulting from harsh oxidative unzipping process, indicating defective states/traps in which the conduction electrons might have been trapped, thereby reducing the mobility values of the ribbons in comparison to pristine graphene.

X-Band Pulse ESR. Pulsed ESR methods use the electron spin–echo (ESE) signal for studying the dynamical behavior of a spin system by observation of the spin system magnetization behavior after a short (ns) microwave pulse excitation. According to our knowledge, pulsed ESR has not been applied so far for the investigation of GNR systems, although it is a very promising local probe that can provide unique information concerning the spin relaxation process. Also, no direct measurement of the spin–lattice relaxation time (T_1) by pulse ESR has been reported for GNRs. In contrast to classical cw ESR, which operates on resolved spectral lines, the ESE methods can resolve the line width of the unresolved homogeneous spin packets that form the inhomogeneously broadened ESR line by measuring the spin–spin/phase memory relaxation time T_2 (T_M). ESE can be excited for inhomogeneously broadened ESR lines only. This allows the immediate differentiation between ESR signals of delocalized spins (conduction electrons, if any) having homogeneously broadened ESR lines and ESR signals of inhomogeneously localized spins.

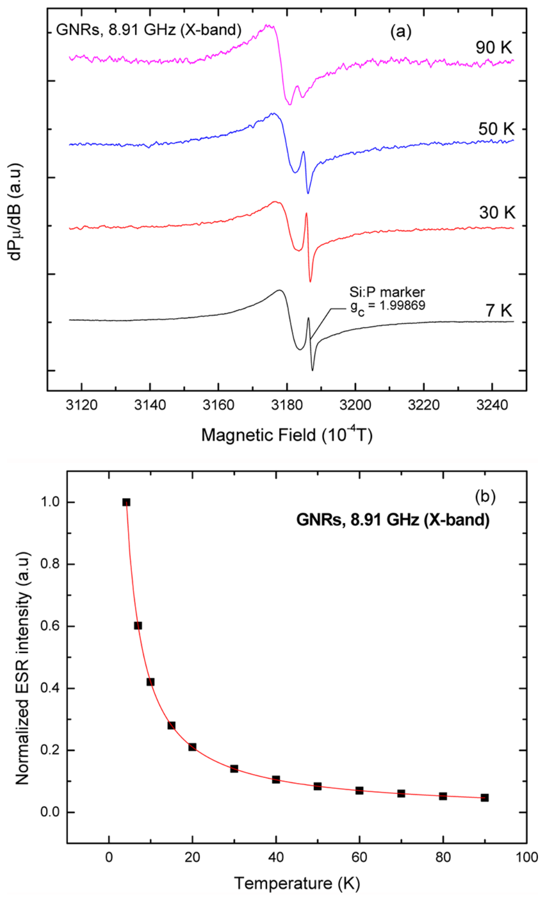

Figure 3. (a) First derivative X-band (~8.91 GHz) ESR spectra measured on GNRs using a modulation field of 0.3 (10^{-4} T) and incident microwave power of 1.3 nW. The signal at $g \sim 1.99869 \pm 0.00002$ stems from a co-mounted Si:P marker sample. (b) Temperature dependence of normalized X-band (~8.91 GHz) ESR intensity measured on GNRs, reflecting the Curie-type behavior; the solid red curve represents the theoretical Curie dependence.

A spin packet is a group of spins having the same resonance Larmor frequency. The various spin packets making up an ESR line differ slightly in this frequency as a consequence of nonresolved (super)hyperfine structure and/or inhomogeneity within the system or the external magnetic field. Because the spin packets are very narrow (typically tens of μ-Tesla), they are very sensitive to molecular and atomic dynamics. Pulse ESR allows the direct observation of the relaxation processes in unpaired electron spin systems. The magnetization of a spin system disturbed by pulse excitation returns to equilibrium in a time of order of seconds at liquid helium temperature and microseconds at room temperature. It is due to spin–lattice relaxation processes. Moreover, microwave pulses at resonance frequency produce coherent precession motion of the electron magnetic moments of spin as the ESE signal decay. The decay rate is sensitive to spin diffusion and spectral diffusion within the spin system and to local motion of the radical center or its surroundings.

Given the non-Lorentzian character of the cw ESR line shape (Figure 1), we decided to perform additional pulsed ESR experiments. Though we did not see two ESR signals even at high frequencies in cw ESR experiments, in pulsed ESR experiments, we found that the ESE signal could be deconvoluted into two components, slower and faster decay components, as discussed below. Figure 4 presents the inversion–recovery and Hahn echo decay traces (shown in black) for GNRs measured at the field position of $B_0 \sim 3300 \times 10^{-4}$ T and at temperature of 20 K. Least-squares double exponential fits are indicated by continuous curves (in red) for both the relaxation processes, that is, spin–lattice (T_1) and spin–spin relaxation times (T_2), using the following equations

$$y = y_0 + A_1 \exp(-2\tau/T_1) + A_2 \exp(-2\tau/T_1) \quad (1)$$

$$y = y_0 + A_1 \exp(-2\tau/T_2) + A_2 \exp(-2\tau/T_2) \quad (2)$$

$$1/T_M = 1/T_2 + 1/T_{ID} \quad (3)$$

where y_0 is the offset in the ESE amplitude, A_1 and A_2 are the pre-exponential factors, T_1 is the spin–lattice relaxation time, T_2 is the spin–spin relaxation time, τ is the time between the pulses, T_M is the phase memory time, and T_{ID} is the time describing the echo decay due to instantaneous diffusion (ID). For the measured spin concentration of 6×10^{19} g^{-1}, and the assumed localization of the paramagnetic centers on the ribbons edges, the instantaneous diffusion cannot be neglected and the measured T_M can be significantly shorter than T_2, hence, T_M is being used. At all of the temperatures covered, the relaxation times are extracted by fitting the corresponding ESE signal by a double exponential decay using the above equations. The temperature dependences for the two components of each relaxation processes are plotted in the Figures 5a,b. The slower component of T_1 decreases with the increase of temperature (cf. Figure 5a) until the temperature of ~75 K, and T_1 is almost constant above this temperature. A similar behavior is observed for the faster component. On the other hand, as shown in Figure 5b, the slower component of T_2 (T_M) increases as a function of temperature until ~100 K and then slowly decreases again with further increase in temperature. The faster component of this process behaves in a similar way but appears to be less temperature dependent. It should be noted that while a two-component decay well describes the experimental data, it is possible that we have a superposition of more than two components.

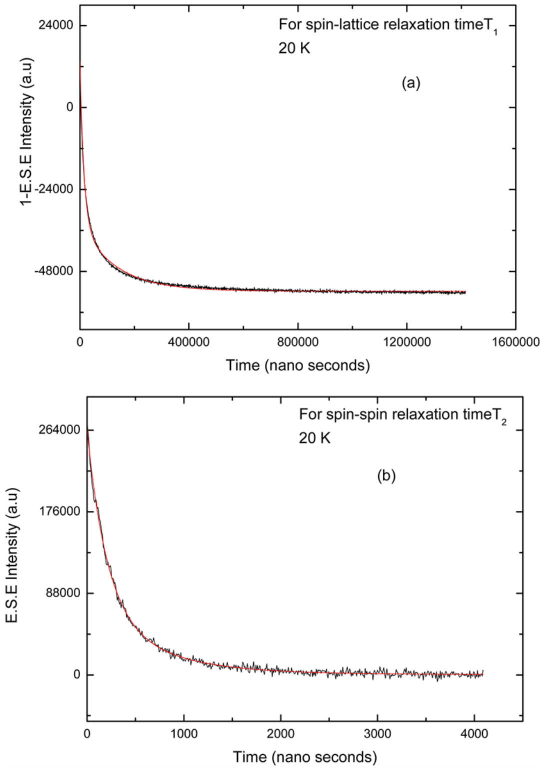

Figure 4. X-band ESR pulse inversion–recovery traces (black) for GNRs measured at the field position $B_0 = 3300 \times 10^{-4}$ T collected at 20 K for the spin–lattice relaxation time (T_1) (a) and for phase memory time (T_M) (b). Least-squares double exponential fits are indicated by red traces. For further details, see the text.

Such a two-component spin relaxation process has been observed earlier[26] in the case of hydrogenated amorphous carbon. In the previous pulsed ESR experiments[27] performed on carbon nanofoam samples, the authors inferred a low temperature T_1 of the order of microseconds, and was shown to be constant above 100 K. To probe the spin dynamics, Clewett and co-authors[28] conducted power saturation ESR studies on MWCNTs to extract temperature-dependent relaxation data. Similar to our observations, they also have reported T_2 on the order of $\approx 660 \pm 50$ ns at all temperatures while T_1 was found to be a strong function of temperature; that is, T_1 is on the order of ≈ 150 μs below 10 K and ≈ 7 μs above 125 K, roughly following an exponential decrease. In a recent systematic study[6] of spin transport in bilayer graphene, long spin relaxation times of 2 ns have been observed at room temperature and are reported to be longer

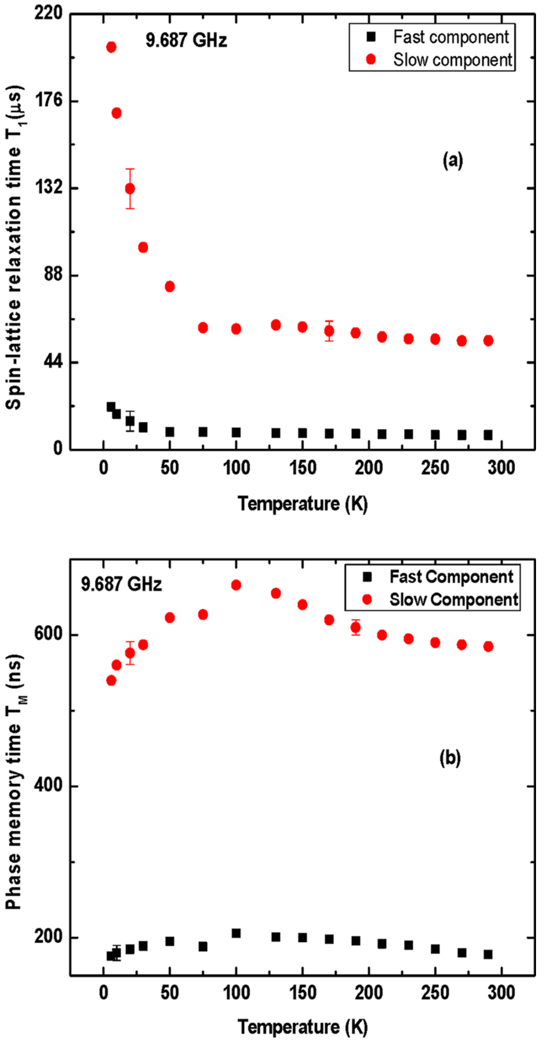

Figure 5. Temperature dependences of the spin−lattice (T_1) (a) and phase memory times (T_M) (b) for both the slow and fast components measured on GNRs.

than those of single-layer graphene, which was attributed to the dominance of D'yakonov-Perel spin scattering in BLG.

From this point on, we will continue our discussion pertaining to the temperature dependence of T_1 derived only from the longer exponential recovery component. Generally, in solids, the temperature dependence of the spin−lattice relaxation (SLR) process can be described by direct, Orbach, and Raman mechanisms.[29] The direct SLR process is linear in temperature and is generally only observed at very low temperature. At higher temperatures, the Raman and/or Orbach processes usually dominate. If a sufficiently large temperature range can be studied, the Raman and Orbach mechanisms can be distinguished from each other on the basis of their different temperature dependencies.

We have tested the applicability of the Raman and Orbach relaxation mechanisms to account for the observed temperature dependence of the spin−lattice relaxation rate in GNRs. As outlined in the Supporting

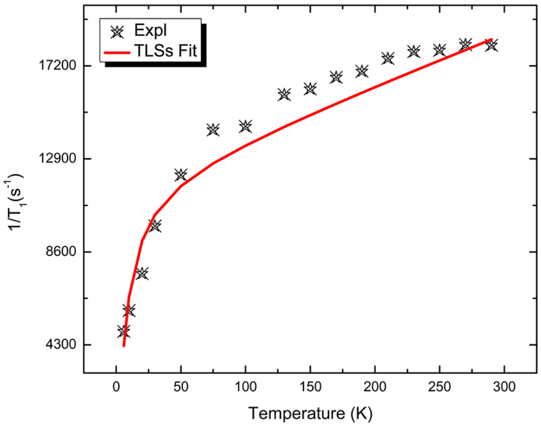

Figure 6. Temperature dependence of the spin−lattice relaxation rate $1/T_1$ for GNRs sample. Shown are the experimental data (symbols) as well as the theoretically generated values (red curve) using the TLS model with a TLS splitting (Δ) of 10 K.

Information, we have found that the temperature dependence of spin relaxation rate may not be ascribed either to the Orbach process or to the Raman process. A search for plausible mechanism has to be sought. Alternatively, we have tested the validity of the TLS model (see below) to describe the temperature dependence of the relaxation rate more adequately. It is pertinent to note that the role of the hyperfine field originating from hydrogen cannot be ruled out as it was shown[30] to play an important role in determining the spin relaxation rate in other organic materials.

Having realized so, we have analyzed our data further using a well-developed and widely tested model for disordered solids such as carbon-derived materials, the so-called two-level tunneling state model as it was elegantly described and reported by Hoffmann's group on various carbon-based systems such as carbon nanoparticles,[31] CO_2^- radiation defects,[32] paramagnetic centers in polymers and in resins[33,34] as well as in the case of noncarbaneous materials.[35]

According to the TLS model, the potential energy surface of a disordered solid contains many shallow asymmetric local minima, which can be approximated by a collection of two-level double wells. Similar to other disordered solids, the relaxation rate $1/T_1$ is relatively fast at low temperatures (as compared to well-ordered solids) and rather slowly increases with temperature. In Figure 6, we plot the variation of the relaxation rate ($1/T_1$) as a function of temperature. This figure includes the experimental data (symbols) as well as the pattern (red curve) generated from the TLS model, given by the equation 4 shown below. We find that our data are in good agreement with the TLS model

$$\frac{1}{T_1} = aT + b\,\mathrm{cosech}\left(\frac{\Delta}{kT}\right) \qquad (4)$$

with parameters $a = 21\ s^{-1}\ K^{-1}$, $b = 1.34 \times 10^4\ s^{-1}$, tunneling level splitting $\Delta = 10$ K, k = Boltzmann constant.

From the above discussion, we may identify the most likely mechanism that accounts for the temperature dependence of spin–lattice relaxation rate in GNRs as TLSs with an orbital level separation is about 10 K.

The temperature dependence of phase memory time T_M shows a rather complex behavior. It first grows up to ~100 K and is observed to slowly decrease with further increase in temperature. While trying to analyze the temperature dependence of phase memory rate ($1/T_M$), we have calculated the spin packet width ΔB_{packet}[31] as a function of temperature from 6 to 100 K. We find that ΔB_{packet} decreases from 76 μT (at 6 K) to 62 μT (at 100 K), which is opposite to the behavior expected for the TLS model.[31] Hence, it appears that the same TLS behavior cannot account for both the temperature dependences of the spin–lattice and the phase-memory relaxation rates. Clearly, further work is needed to arrive at a complete picture.

Now, we estimate the homogeneous line width from phase-memory relaxation time $T_M = 1/(\gamma \times \Delta B_{PP})$ measured at 10 K at X-band frequency, where γ is the gyromagnetic ratio and T_M = 560 ns at 10 K. The homogeneous line width is obtained as 0.2×10^{-4} T, which obviously cannot account for the measured X-band line width of $\sim 6 \times 10^{-4}$ T at 10 K (cf. Figure 2). Therefore, the remaining line width must arise from inhomogenous broadening. Hence, the pulsed ESR data tell us that the existence of the ESE signal in GNRs is evidence that the ESR line is inhomogeneously broadened. This indicates that the unpaired spins are localized in the GNRs. At this juncture, two questions arise: (1) What is the reason for the inhomogeneous broadening, that is, what is the origin of spin packets forming the ESR line? Two possibilities can be considered. ESR g factors can be slightly different for radical centers located at different sites of GNRs. Such dispersion in g value is generally observed in disordered and amorphous solids and has been observed in coal samples also. It seems that a small g factor dispersion can take place in nanographitic units of GNRs. The second possibility is related to dangling bonds on the peripheries of the GNRs. These bonds are practically saturated and it can be caused, at least partially, by attaching hydrogen atoms during GNR preparation. Hyperfine coupling between unpaired electron spins and hydrogen nuclei will produce inhomogeneous broadening of the ESR line. In GNRs, both scenarios appear to be present. The latter possibility can be seen from our results of HYSCORE experiments, reported in our earlier work.[15] (2) A more fundamental question is related to the origin of unpaired spin states in GNRs. There is still no definite answer to this question. Five different structural defects can be considered as responsible for unpaired electron creation: (a) dangling σ bonds on the edges of graphene sheets; (b) a defect in the form of an adatom, which can be a carbon atom lying on a graphene plane and bridging a carbon–carbon bond on the graphene surface; (c) a carbon vacancy formed by removing a carbon atom from the graphene sheet and relaxing to a pentagon structure during the splitting process; (d) sterically protected carbon radicals that are immobilized in the aromatic system of sp^2-bonded carbons; and (e) localized nonbonding π-electron states at zigzag graphene edges. However, from the presence of the strong ESR signal detected on GNRs stored in open air, one may exclude the possible contribution of carbon vacancies.

SUMMARY AND CONCLUSIONS

In the present work, we have addressed several relevant items regarding the nature and dynamics of spin states in GNRs using broad-band ESR spectroscopy. The salient features of this study include the following: (a) The multifrequency cw ESR data indicate the presence of only carbon-related paramagnetic nonbonding states, at any measured temperature, where the g value (g = 2.0032) is independent of microwave frequency and temperature. (b) A linear broadening of ESR signal as a function of microwave frequency is detected, which is ascribed to the presence of a distribution in g factors, also causing the non-Lorentzian line shape. However, this inhomogeneous broadening is found to be rather small; the large contribution may come from unresolved hyperfine interaction arising from hydrogen. (c) The electron spin–lattice relaxation process is found to be characterized by slow and fast components, whose temperature dependence could be well-described by a TLS-type relaxation mechanism. The present experimental work may help to advance the present understanding on the edge spin (or magnetic)-based properties of GNRs.

EXPERIMENTAL SECTION

Briefly, K-split GNRs were synthesized by sealing MWCNTs with an outside diameter of 40–80 nm and approximately 15–20 inner nanotube layers in a glass tube with metallic potassium, and the tube was heated in a furnace at 250 °C for 14 h, followed by quenching in ethanol. Upon sonication in chlorosulfonic acid, the split MWCNTs were further exfoliated to form GNRs. This procedure[11] is known to produce GNRs that are free from oxidative damage, with conductivities paralleling the properties of the best samples of mechanically exfoliated graphene. Scanning electron microscopy (SEM) and atomic force microscopy (AFM) images indicated GNRs with widths of 130–250 nm and a length of 1–5 μm. Several techniques were used to fully characterize GNRs and to test their electronic properties, as published elsewhere.[11]

Conventional first derivative cw ESR spectra were taken at three different "low" microwave frequencies: X- (~8.91 GHz), K- (~20.6 GHz), and Q-band (~34.0 GHz), operated in the temperature range of 4.2−300 K using locally constructed X- and K-band spectrometers (providing the best sensitivity at low temperature) and a commercial X-band Jeol JES-FA 100 and a commercial Bruker EMX spectrometer. Depending on the observational temperature, X-band observations were made using either the JEOL JES-FA 100 spectrometer (room temperature investigations) or the locally designed instrument optimized for low-temperature measurements. All four spectrometers were driven in the adiabatic mode, equipped with a cylindrical TE$_{011}$ microwave reflection cavity. Routinely, conventional cw low-power first derivative absorption (dP_μ/dB, P_μ being the applied microwave power) spectra were detected by applying sinusoidal modulation (∼100 kHz; amplitude $B_m \geq 0.08 \times 10^{-4}$ T) of the externally applied static magnetic field $\boldsymbol{B}$. Defect densities were determined through double numerical integration of the detected dP_μ/dB signals using a co-mounted (point-like) reference sample. Depending on spectral composition and/or the ESR parameter aimed to isolate, various types of markers were used. Mostly, this was a Si:P marker[18] (electron spin $S = 1/2$, $g = 1.99869 \pm 0.00002$ at 4.2 K) which was used.

High-frequency ESR experiments were performed at 239.2 and 336 GHz using the quasioptical spectrometer that has been developed at the National High Magnetic Field Laboratory (NHMFL). This setup was a superheterodyne spectrometer, employing a quasioptical submillimeter bridge, and operated in the reflection mode without cavity, with a sweepable 12.5 T superconducting magnet.[19] The incident power on the sample was about 20 μW. The pulse ESR experiments were performed using a Bruker Elexsys-580 X-band pulse ESR spectrometer, which was equipped with an CF935 flow cryostat. To record field-swept echo (FSE) ESR spectra and to measure the spin−spin relaxation time T_2 or phase memory time (T_M), the two-pulse $\pi/2$-τ-π-τ-echo Hahn echo sequence was used (sequence 1), while the electron spin−lattice relaxation time T_1 was measured by the inversion−recovery π-t-$\pi/2$-τ-π-τ-echo pulse sequence (sequence 2). In both cases, the lengths of the microwave $\pi/2$ and π pulses were 32 and 64 ns, respectively, and the entire echo was integrated. The pulse duration was experimentally chosen to obtain full saturation and maximal echo amplitude. All ESR experiments presented in this work have been performed on GNRs stored in open air ambient.

Conflict of Interest: The authors declare no competing financial interest.

Acknowledgment. The National High Magnetic Field Laboratory is supported by NSF Cooperative Agreement No. DMR-0654118, and by the State of Florida. The work at Rice University was supported by the Air Force Office of Scientific Research FA9550-09-1-0581 and the Office of Naval Research MURI Graphene program.

Supporting Information Available: Applicability of Lorentzian and Gaussian line shape fittings to the observed ESR signal measured from GNRs, are shown in Figures S1 and S2. Figure S3 describes the temperature dependence of the Q-band ESR line width (ΔB_{PP}). In Figure S4, the applicability of Orbach and Raman relaxation processes is shown to describe the temperature variation of electron spin−lattice relaxation rate, together with the discussion and relevant references. This material is available free of charge *via* the Internet at http://pubs.acs.org.

REFERENCES AND NOTES

1. Novoselov, K. S.; Geim, A. K.; Morozov, S. V.; Jiang, D.; Zhang, Y.; Dubonos, S. V.; Grigorieva, I. V.; Firsov, A. A. Electric Field Effect in Atomically Thin Carbon Films. *Science* **2004**, *306*, 666–669.
2. Soriano, D.; Muñoz-Rojas, F.; Fernández-Rossier, J.; Palacios, J. J. Hydrogenated Graphene Nanoribbons for Spintronics. *Phys. Rev. B* **2010**, *81*, 165409–165416.
3. Yazyev, O. V. Magnetism in Disordered Graphene and Irradiated Graphite. *Phys. Rev. Lett.* **2008**, *101*, 037203–037207.
4. Tombros, N.; Jozsa, C.; Popinciuc, M.; Jonkman, H. T.; van Wees, B. J. Electronic Spin Transport and Spin Precession in Single Graphene Layers at Room Temperature. *Nature* **2007**, *448*, 571–574.
5. Shimizu, T.; Haruyama, J.; Marcano, D. C.; Kosinkin, D. V.; Tour, J. M.; Hirose, K.; Suenaga, K. Large Intrinsic Energy Bandgaps in Annealed Nanotube-Derived Graphene Nanoribbons. *Nat. Nanotechnol.* **2010**, *249*, 45–50.
6. Yang, T. Y.; Balakrishnan, J.; Volmer, K.; Avsar, A.; Jaiswal, M.; Samm, J.; Ali, S. R.; Pachoud, A.; Zeng, M.; Popinciuc, M.; *et al.* Observation of Long Spin-Relaxation Times in Bilayer Graphene at Room Temperature. *Phys. Rev. Lett.* **2011**, *107*, 047206–047210.
7. Han, W.; Wang, W. H.; Pi, K.; McCreary, K. M.; Bao, W.; Li, Y.; Miao, F.; Lau, C. N.; Kawakami, R. K. Electron-Hole Asymmetry of Spin Injection and Transport in Single-Layer Graphene. *Phys. Rev. Lett.* **2009**, *102*, 137205–137209.
8. Józsa, C.; Popinciuc, M.; Tombros, N.; Jonkman, H. T.; van Wees, B. J. Electronic Spin Drift in Graphene Field-Effect Transistors. *Phys. Rev. Lett.* **2008**, *100*, 236603–236607.
9. Ertler, C.; Konschuh, S.; Gmitra, M.; Fabian, J. Electron Spin Relaxation in Graphene: The Role of the Substrate. *Phys. Rev. B* **2009**, *80*, 041405–041409.
10. Simon, F.; Muranyi, F.; Dora, B. Theory and Model Analysis of Spin Relaxation Time in Graphene—Could It Be Used for Spintronics? *Phys. Status Solidi B* **2011**, *248*, 2631–2634.
11. Kosynkin, D. V.; Lu, W.; Sinitskii, A.; Pera, G.; Sun, Z.; Tour, J. M. Highly Conductive Graphene Nanoribbons by Longitudinal Splitting of Carbon Nanotubes Using Potassium Vapor. *ACS Nano* **2011**, *5*, 968–974.
12. Kosynkin, D. V.; Higginbotham, A. L.; Sinitskii, A.; Lomeda, J. R.; Dimiev, A.; Price, B. K.; Tour, J. M. Longitudinal Unzipping of Carbon Nanotubes To Form Graphene Nanoribbons. *Nature* **2009**, *458*, 872–876.
13. Rao, S. S.; Stesmans, A.; Keunen, K.; Kosynkin, D. V.; Higginbotham, A.; Tour, J. M. Unzipped Graphene Nanoribbons as Sensitive O$_2$ Sensors: Electron Spin Resonance Probing and Dissociation Kinetics. *Appl. Phys. Lett.* **2011**, *98*, 083116–083119.
14. Rao, S. S.; Stesmans, A.; Kosynkin, D. V.; Higginbotham, A.; Tour, J. M. Paramagnetic Centers in Graphene Nanoribbons Prepared from Longitudinal Unzipping of Carbon Nanotubes. *New J. Phys.* **2011**, *13*, 113004–113013and references therein.
15. Rao, S. S.; Jammalamadaka, S. N.; Stesmans, A.; Moshchalkov, V. V.; van Tol, J.; Kosynkin, D. V.; Higginbotham, A.; Tour, J. M. Ferromagnetism in Graphene Nanoribbons: Split *versus* Oxidative Unzipped Ribbons. *Nano Lett.* **2012**, *12*, 1210–1217.
16. Matsubara, K.; Tsuzuku, T.; Sugihara, K. Electron Spin Resonance in Graphite. *Phys. Rev. B* **1991**, *44*, 11845–11851.
17. Zaka, M.; Ito, Y.; Wang, H.; Yan, W.; Robertson, A.; Wu, Y. A.; Rümmeli, M. H.; Staunton, D.; Hashimoto, T.; Morton, J. J. L.; *et al.* Electron Paramagnetic Resonance Investigation of Purified Catalyst-Free Single-Walled Carbon Nanotubes. *ACS Nano* **2010**, *4*, 7708–7716.
18. Stesmans, A. Structural Relaxation of Pb Defects at the (111)Si/SiO$_2$ Interface as a Function of Oxidation Temperature: The Pb-Generation—Stress Relationship. *Phys. Rev. B* **1993**, *48*, 2418–2436.
19. van Tol, J.; Brunel, L. C.; Wylde, R. J. A Quasioptical Transient Electron Spin Resonance Spectrometer Operating at 120 and 240 GHz. *Rev. Sci. Instrum.* **2005**, *76*, 074101–074109.
20. Kurganova, E. V.; van Elferen, H. J.; McCollam, A.; Ponomarenko, L. A.; Novoselov, K. S.; Veligura, A.; van Wees, B. J.; Maan, J. C.; Zeitler, U. Spin Splitting in Graphene Studied by Means of Tilted Magnetic-Field Experiments. *Phys. Rev. B* **2011**, *84*, 121407–121411.
21. Olariu, A.; Náfrádi, B; Ćirić, L; Nemes, N. M.; Forro, L. High Frequency Electron Spin Resonance Study of Peapods. *Phys. Status Solidi B* **2008**, 1–5.
22. Blinc, R.; Cevc, P.; Arčon, D.; Zalar, B.; Zorko, A.; Apih, T.; Milia, F.; Madsen, N. R.; Christy, A. G.; Rode, A. V. ^{13}C NMR and EPR of Carbon Nanofoam. *Phys. Status Solidid B* **2006**, *243*, 3069–3072.

23. Elliot, R. J. Theory of the Effect of Spin−Orbit Coupling on Magnetic Resonance in Some Semiconductors. *Phys. Rev.* **1954**, *96*, 266–279.
24. Ishii, S.; Miyamoto, K.; Oguri, N.; Horiuchi, K.; Sasaki, T.; Aoki, N.; Ochiai, Y. Conduction Carriers in Multi-Walled Carbon Nanotubes. *Physica E* **2003**, *19*, 149–152.
25. Beuneu, F.; l'Huillier, C.; Salvetat, J. P.; Bonard, J. M.; Forro, L. Modification of Multiwall Carbon Nanotubes by Electron Irradiation: An ESR Study. *Phys. Rev. B* **1999**, *59*, 5945–5949.
26. Blinc, R.; Arčon, D.; Cevcy, P.; Pocsikz, I.; Koosz, M.; Trontelj, Z.; Jaglicic, Z. ^{13}C Nuclear Magnetic Resonance and Electron Spin Resonance of Amorphous Hydrogenated Carbon. *J. Phys.: Condens. Matter* **1998**, *10*, 6813–6824.
27. Arčon, D.; Jagličič, Z.; Zorko, A.; Rode, A. V.; Christy, A. G.; Madsen, N. R.; Gamaly, E. G.; Luther-Davies, B. Origin of Magnetic Moments in Carbon Nanofoam. *Phys. Rev. B* **2006**, *74*, 014438–014447.
28. Clewett, C. F. M.; Li, P.; Pietrass, T. Electron Spin Resonance Studies of Hydrogen Adsorption on Defect-Induced Carbon Nanotubes. *J. Phys. Chem. C* **2007**, *111*, 6263–6267.
29. Kulik, L. V.; Lubitz, W.; Messinger, J. Electron Spin−Lattice Relaxation of the S_0 State of the Oxygen-Evolving Complex in Photosystem II and of Dinuclear Manganese Model Complexes. *Biochemistry* **2005**, *44*, 9368–9374and references therein.
30. Robbert, P. A. Organic Semiconductors: What Makes the Spin Relax? *Nat. Mater.* **2010**, *9*, 288–290.
31. Lijewski, S.; Wencka, M.; Hoffmann, S. K.; Kempinski, M.; Kempinski, M.; Bartkowiak, M. S. Electron Spin Relaxation and Quantum Localization in Carbon Nanoparticle: Electron Spin Echo Studies. *Phys. Rev. B* **2008**, *77*, 014304–014312.
32. Wencka, M.; Lijewski, S.; Hoffmann, S. K. Dynamics of CO^{-}_{2} Radiation Defects in Natural Calcite Studied by ESR, Electron Spin Echo and Electron Spin Relaxation. *J. Phys.: Condens. Matter* **2008**, *20*, 255237–255247.
33. Hoffmann, S. K.; Hilczer, W.; Goslar, J.; Kiczka, S.; Polus, I. Resonance-Type Effects in Free Radical Electron Spin−Lattice Relaxation and Electron Spin Echo Dephasing Due to a Dynamics of a Homogeneous-Chain Oligomeric System. *Phys. Chem. Chem. Phys.* **2002**, *4*, 4944–4951.
34. Hoffmann, S. K.; Hilczer, W.; Radczyk, T. Electron Spin-Lattice Relaxation in Polymers and Crystals Related to Disorder and Structure Defects. *Acta Phys. Pol., A* **2003**, *103*, 373–385.
35. Hoffmann, S. K.; Goslar, J.; Lijewski, S. Suppression of Raman Electron Spin Relaxation of Radicals in Crystals. Comparison of Cu^{2+} and Free Radical Relaxation in Triglycine Sulfate and Tutton Salt Single Crystals. *J. Phys.: Condens. Matter* **2011**, *23*, 345403–345414.